CHALMERS
UNIVERSITY OF TECHNOLOGY

$$\frac{\partial n_j}{\partial t} + \nabla \cdot (n_j \vec{v}_j) = 0$$

$$m_j n_j \frac{\partial \vec{v}_j}{\partial t} + m_j n_j \vec{v}_j \cdot \nabla \vec{v}_j = n_j q_j (\vec{E} + \vec{v}_j \times \vec{B}) - \nabla p_j - \nabla \cdot \pi_j$$

$$\frac{\partial}{\partial t}\left(\frac{1}{2} m_j n_j v_j^2 + \frac{3}{2} p_j\right) + \nabla \cdot \left[\left(\frac{1}{2} m_j n_j v_j^2 + \frac{5}{2} p_j\right)\vec{v}_j + \pi_j \cdot \vec{v}_j + \vec{q}\right] = q_j n_j \vec{E} \cdot \vec{v}_j$$

$$\nabla \cdot \vec{E} = \frac{\rho}{\epsilon_0} \qquad \nabla \times \vec{E} = -\frac{\partial \vec{B}}{\partial t}$$

$$\nabla \cdot \vec{B} = 0 \qquad \nabla \times \vec{B} = \frac{1}{c^2}\frac{\partial \vec{E}}{\partial t} + \frac{1}{c^2 \epsilon_0}\vec{J}$$

Turbulent transport in fusion plasmas

Master’s thesis

Ken Ryrbo

Department of Earth and Space Sciences
CHALMERS UNIVERSITY OF TECHNOLOGY
Gothenburg, Sweden 2015

Master's thesis 2015:NN

Turbulent transport in fusion plasmas

Ken Ryrbo

Department of Earth and Space Sciences
Plasma Physics and Fusion Energy
Chalmers University of Technology
Gothenburg, Sweden 2015

Abstract

In order to improve the confinement time for tokamak type fusion reactors the nature of turbulent transport in fusion plasmas needs to be better understood. In this thesis the transport predicted by an advanced fluid model, called the Weiland model, will be investigated analytically to further the understanding of which factors contribute to both inward and outward transport in various circumstances. The analytical expressions are then used to investigate how the flux of particles and heat relate to the density and temperature gradients in the plasma.

Keywords: Fusion, plasma physics, tokamak, peaking factor, ITG, TEM.

Acknowledgements

First and foremost I would like to thank my supervisor, professor Hans Nordman, for giving me the opportunity to delve deeper into the world of fusion and for providing guidance, insight and many interesting discussions along the way. I would also like thank Marcus Eriksson for peaking my interest in renewable energy and for the many walks around campus where we exchanged thoughts and ideas. Finally I would like to thank Svea for making me want to make the future a better place.

Nomenclature

Most of the reoccurring abbreviations and symbols are described here. Note that we write $\nabla = \partial_x = \frac{\partial}{\partial x}$ below.

Symbols

Inverse gradient length $L_f = -\frac{f}{\nabla f}$
Cyclotron frequency $\omega_c = \frac{|q|B}{m}$
Larmor radius $\rho = \frac{v_\perp}{\omega_c}$
Fraction of trapped electrons f_t
$\epsilon_n = \frac{2L_n}{L_B}$
$\eta_j = \frac{L_{n_j}}{L_{T_j}}$
$\tau = \frac{T_e}{T_i}$
$\omega_{Dj} = 2\frac{k_\perp T_j}{qB}\frac{\nabla B}{B}$
$N_j = \omega^2 - \frac{10}{3}\omega\omega_{Dj} + \frac{5}{3}\omega_{Dj}^2$
$\hat{N}_j = N_j/\omega_{De}^2$
$\hat{\omega} = \omega/\omega_{De}$

Abbreviations

ITG Ion Temperature Gradient
TEM Trapped Electron Mode

Contents

Introduction **1**
The need for clean and safe energy 1
Topics covered 2

1 Fusion and plasma physics **3**
1.1 The nucleus and nuclear reactions. 3
Where does the energy come from? 4
Overcoming the Coulomb barrier 4
1.2 Plasmas 5
1.3 Fusion plasmas and tokamaks 5
Transport in tokamaks 7

2 Kinetic and fluid modeling of plasmas **9**
2.1 The distribution function 9
The Vlasov equation 10
Moments of the Vlasov equation 11
2.2 The Weiland fluid model 11

3 Particle transport **13**
3.1 Particle flux 13
3.2 The peaking factor 14
Peaking factors for various $\hat{\omega}_r$ and $\hat{\gamma}$ 15
3.3 Pellet fueling application 16

4 Simulations **19**
4.1 Particle flux in pellet fueled plasmas 19
4.2 Peaking factors 23
ITG mode dominated plasmas 23
TE mode dominated case 25

Summary and conclusions **27**
Possible future work 27

A Derivations **31**
Finding $\hat{\omega} = \hat{\omega}_r + i\hat{\gamma}$ from quasi-neutrality 31
The ITG mode 32
The TE mode 33

B Flux calculations **35**
Ion heat flux 35
    Positive and negative contributions to χ_i 36
    Ion heat flux 36
    Peaking factors 37
Electron heat flux 37
    Positive and negative contributions to χ_e 38
    Electron heat flux 38
    Peaking factors 38

C Basic particle motion due to electric and magnetic fields **41**
    Contributions to particle drift in tokamaks 42

Introduction

The need for clean and safe energy

The increased demand for energy coupled with the ambition to decrease the environmental impact resulting from the use of fossil fuel makes it necessary to seek out new non-polluting alternatives to such energy sources as oil, coal and traditional nuclear power. Such alternatives in current use include solar, wind and hydroelectric power. In the case of solar and wind power, their variation in energy output makes them unsuitable to replace the need for energy stemming from large energy consumers such as industris and huge cities. They will however work very well as a complement, coupled with general energy conservation, in providing energy locally on a smaller scale.

Hydroelectric power is a more stable source of energy but its utility varies greatly depending on different countries access to huge bodies of flowing water. Sweden, for example, gets around 45% of its base energy from hydroelectric power, while the number for the Unites States is 9%, and for the world overall around 2%[1].

Fusion as an energy source has great potential to be a key component for future sustainable energy production. Since the energy produced stems from nuclear reactions rather than chemical, which is the case for oil and coal, it is estimated to release approximately one million times more energy per reaction. This means that the amount of fuel for producing the same amount of energy is greatly decreased. It is estimated that we have fairly easy access to over 20 000 years of inexpensive fuel on earth needed for the *deuterium-trituim* reaction that is projected to be the fusion reaction used for the first generation of fusion power plants. In time, the more difficult to induce *deuterium-deuterium* reaction is hoped to be used, extending the availability of fuel to billions of years as deuterium can be easily extracted from ordinary sea water, while tritium must be created continuously from lithium due to the fact that tritium is radioactive with a relatively short half-life of 12 years.

Besides the benefit of producing huge amounts of energy a fusion reactor would have several other benefits. First of all, there are no CO_2 emissions whatsoever, nor any other chemically reactive substances, since the main rest product from the deuterium-tritium reaction would be regular chemically inert helium ^{4}He. There would be some radioactive material due to the wall of the reactor being activated by high energy neutrons, that would need to be stored for some time, but the time scale would be much shorter than that of traditional nuclear waste. Further, since the fusion reactor would not depend on chain reactions between the nuclei, as is the case for current nuclear power plants, the risk of an accelerated reaction resulting in a possible meltdown would be removed.

---

[1] See [1], chapter 1.

However, the construction of a fusion reactor is not without its obstacles. In order to induce a sustained fusion reaction a fusion plasma must be created and heated to over 10^8 K while being held in place by a magnetic field so that particles keep fusing and not diffuse out of the plasma core and thus ending the sustained reaction. The main focus on this thesis is to model the heat and particle flux in a magnetically confined plasma given by an analytical treatment of the Weiland model, an advanced fluid model developed at Chalmers.

Topics covered

Main topics dealt with are:

Chapter 1: We give a brief introduction to nuclear fusion reactions and some basic plasma physics needed in order to understand how fusion plasmas work. We also describe the Tokamak, which is currently the most viable option for being the first fusion reactor to achieve sustained ignition through magnetic confinement.

Chapter 2: The approach of kinetic modelling of plasmas is introduced and we derive the fluid equations used for describing a fusion plasma. The assumptions of the so called Weiland model, which is a successful model of fusion plasmas developed at Chalmers, are described and some of the most important results are given.

Chapter 3: We treat earlier know results of the Weiland model analytically in order to better see what dependencies the flux of particles and heat have. We also intoduce the concept of the peaking factor and present a possible application of the model relevant to a method of injecting fuel into the reactor, called pellet fueling.

Chapter 4: Using the equations for particle flux we use Matlab in order to investigate the relation between the particle density gradient and the particle flux. In this process we also find values for the peaking factors and how they relate to various conditions.

Summary and conclusions: A recap of results and suggestions for further study.

Appendix A: Derivation of the ITG and TE modes from quasi-neutrality.

Appendix B: Calculation of the heat fluxes and related peaking factors made in the same way as we calculated the particle flux in chapter 3.

Chapter 1

Fusion and plasma physics

1.1 The nucleus and nuclear reactions.

The atomic nucleus consists of positively charged protons and uncharged neutrons. The number of protons Z determines the element of the atom, while the number of neutrons N can vary slightly, giving rise to different isotopes of the same element. For example, the simplest element hydrogen has in its basic form $Z = 1$ and $N = 0$, but also has naturally occuring isotopes with $N = 1$ and $N = 2$, called *deuterium* D and *tritium* T respectively.

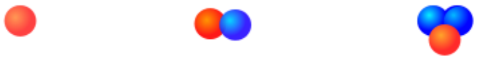

Figure 1.1: Hydrogen, deuterium and tritium nuclei.

The nucleus is held together by the strong nuclear force, counteracting the Coulomb repulsion resulting from the positively charged protons. This strong residual force dominates shorter length scales than the electromagnetic Coulomb forces in play due to the fact that its force carrying particles are much more massive, resulting in the strong force's potential being approximately $\propto \frac{1}{re^r}$, while the Coulomb potential is $\propto \frac{1}{r}$.

This results in some nuclear configurations being unstable. When the distance between two charged particles in the nucleus grows too big the Coulomb repulsion becomes too large for the strong force to counteract and the nucleus breaks apart. This process is called *fission* and is the process used in traditional nuclear power plants. The reverse scenario when a charged particle gains enough momentum to break through the coulomb barrier to the point where the strong force takes over and the particle is absorbed by the nucleus is called *fusion*, and is currently the subject of much research.

Where does the energy come from?

One finds that, if weighed, the nucleus actually has more total mass than the sum of the masses of the particles of which it consists. This is due to the fact that the energy binding the nucleons together gives the nucleus additional energy through the equivalency of mass and energy given by Einsteins famous equation $E = mc^2$. A way to quantify the energy stored in a nucleus is by measuring the binding energy per nucleon. If $A = Z + N$ is the number of nucleons then the binding energy per nucleon, usually measured in MeV, is $\frac{\Delta mc^2}{A}$, where Δm is the difference in mass between the individual nucleons and the nucleus.

An example of a nuclear reaction is

$$\mathrm{D} + \mathrm{T} \to \mathrm{n} + {}^4\mathrm{He} + 17.6\ \mathrm{MeV}$$

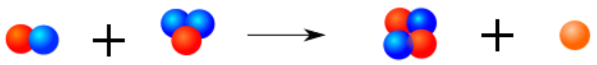

Figure 1.2: Deuterium-tritium fusion resultning in an alpha particle and a free neutron.

where the energy comes in the form of kinetic energy for the alpha particle and the neutron. The reaction above is in fact the reaction intended for use in near future fusion power plants.

Overcoming the Coulomb barrier

As mentioned above, a fusion reaction takes place when two nucleons or nuclei overcome the Coulomb barrier and get close enough to each other for the strong nuclear force to become stronger than the electromagnetic force of repulsion. As seen in figure (1.3), the momentum of the incoming particle must be large enough, otherwise the particle will have its trajectory altered too much and will pass outside the area σ where the strong force would have absorbed it into the nucleus. In order for this to happen on a large enough scale to extract energy of any useful amount the number of collisions per volume needs to be large and thus also the temperature. A measure often used as a benchmark for fusion reactors is the *triple product* $n_j T_j \tau_{E_j}$, where n_j is the particle density, T_j is the temperature and τ_{E_j} is the energy confinement time, all for species j. In order to achieve a sustained ongoing fusion reaction it has been calculated that we must have

$$n_j T_j \tau_{E_j} \gtrsim 3 \cdot 10^{21} \mathrm{m}^{-3} \mathrm{keVs}$$

a value that so far has not been reached in any current experiment. The energy confinements time τ_{E_j} is inversely proportional to the particle and heat transport out of the plasma which motivates further investigation into the physics of transport, which is the main focus of this thesis.

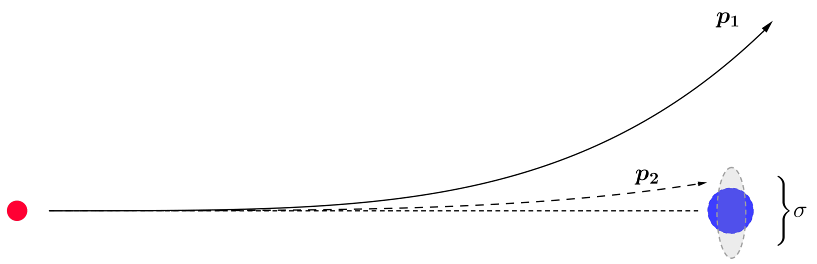

Figure 1.3: An incoming particle might be diverted or absorbed by the nucleus depending on its momentum p_1 or p_2, where $p_2 > p_1$

1.2 Plasmas

Plasma is commonly known as the fourth state of matter, and is as far as we can tell the most common state of ordinary matter in the observable universe. Stars are mostly made up of plasma and in them fusion processes occur, creating heavier elements that are eventually spread across the cosmos as the star dies. Examples of plasmas closer to earth are lightning bolts and aurora, as well as plasmas used in industrial applications. Our interest in plasmas comes from the fact that it is in this state nuclear fusion occurs.

A plasma can be said to be a quasi-neutral gas consisting of freely moving charged ions and electrons, which exhibit collective behavior. What we mean by quasi-neutral is that the number of positive and negative charges in the plasma is approximately equal on a macroscopic level. We express this as

$$n_e \approx n_i \tag{1.1}$$

where n_e is the number of electrons and n_i is the number of ions, in this case assuming that $Z = 1$. The collective behavior mentioned results from the fact that the plasma always tries to even out any regions giving an electric field due to an excess of positive or negative charge in the area. This also means that the plasma is very effective at blocking out electrical fields, a phenomenon known as Debye shielding.

1.3 Fusion plasmas and tokamaks

In order for fusion reactions of hydrogen to occur on any large scale the thermal energy needs to be on the order of hundreds of millions of degrees kelvin. This process occurs naturally in the centers of stars such as our sun due to gravitational pressure and light elements are turned into heavier ones. Since we do not have such great gravitational pressure at our disposal on Earth we need to contain fusion plasmas using the electromagnetic force in machines such as tokamaks and stellarators, of which the tokamak is currently the focus of most research. A tokamak is a torus-shaped device with a **B** field running along its azimuthal direction, which we shall call $\hat{z}$. The reason that a torus shape is used is that it allows for field lines without endpoints. The field lines are twisted in order to confine the plasma in the center of the torus, thus reducing additional drifts of particles. The plasma is heated to an operating temperature above 10 keV, i.e. over 10^8 K , by using a combination of ohmic heating, neutral-beam injection and radio frequency heating.

For a tokamak the Q-value is defined as the ratio between the outgoing and incoming power in the experiment. For $Q = 1$ we would have break-even and for a sustainable working fusion reactor we would need $Q >> 1$.

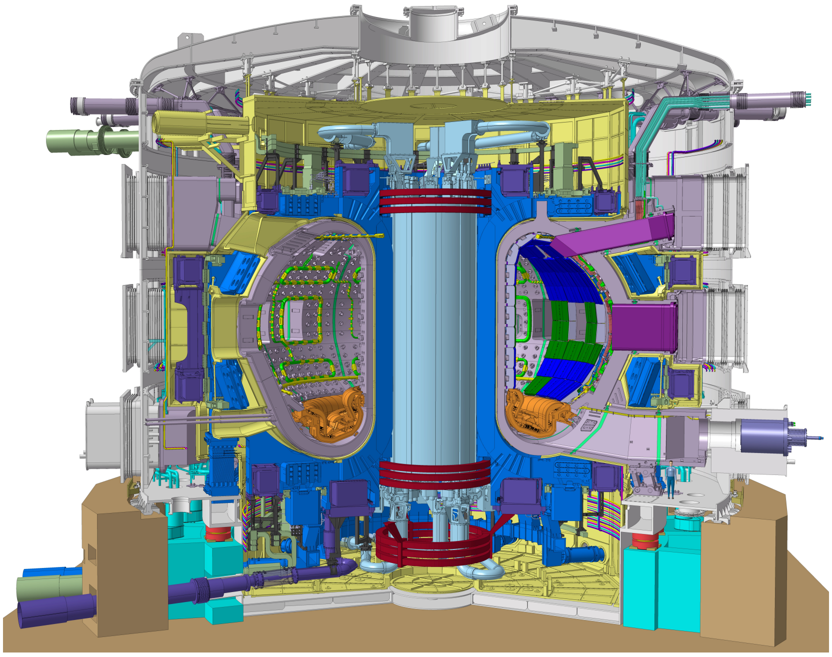

Figure 1.4: Cutaway of the ITER tokamak currently under construction at Cadarache, France. Image taken from *iter.org*

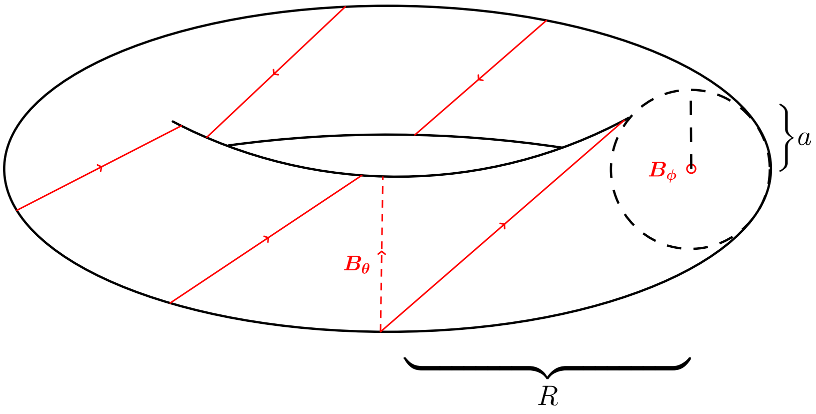

Figure 1.5: A tokamak with major radius R and minor radius a. The twisted **B** field is constructed as the sum of a toroidal and an azimuthal magnetic field.

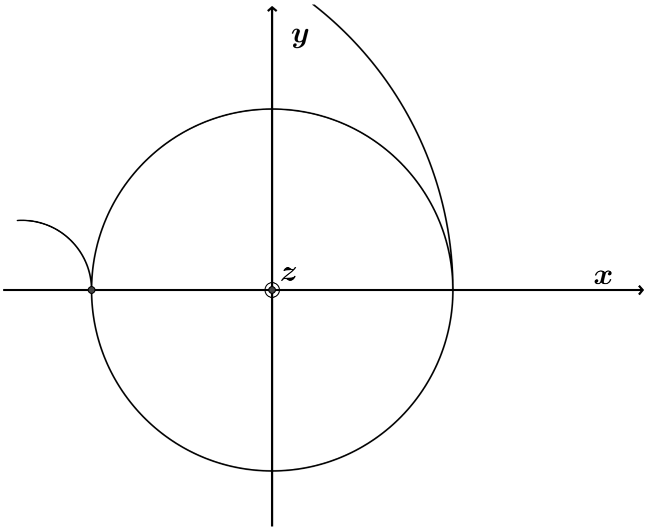

Figure 1.6: Coordinate designation in a tokamak

Transport in tokamaks

Although the plasma is ideally held in place by the twisted magnetic field in the tokamak, particles tend to deviate from the magnetic field lines due to various drift effects such as the centrifugal force, polarization and inhomogeneity of the magnetic field. These effects are described in more detail in appendix C. One usually separates the transport into two categories, where the transport due to collisions is called *classical*, while all other transport is collectively called *anomalous*. It has been found that anomalous transport is the dominant form of transport in tokamaks and thus a major contribution to a lowered energy confinement time. The anomalous transport is caused by small scale fluctuations in the plasma, driven by plasma instabilities.

Chapter 2

Kinetic and fluid modeling of plasmas

The large number of individual particles in a plasma makes detailed calculations very difficult, even with the aid of super computors, so we thus turn to a statistical method known as kinetic theory to make calculations more manageable. We first introduce the notion of a distribution function and then define various physical quantities in terms of this distribution function and see how they relate to each other by imposing restrictions such as continuity, leading to the Vlasov equation.

As the distribution function will depend on 7 variables we use the method of taking moments of the equation, leading to a reduced set of variables needed to describe the position of the resulting quantities. This will give us the fluid equations known as the Braginskii equations, which we will use as our basis for a two-fluid theory describing the motions of electrons and ions within the plasma.

2.1 The distribution function

We define the distribution function $f_j(\mathbf{r}, \mathbf{w}, t)$ by letting $f_j(\mathbf{r}, \mathbf{w}, t) d\mathbf{r} d\mathbf{w}$ be the probability of finding particles of type j within the six-dimensional volume element $d\mathbf{r}d\mathbf{w} = d^3 r d^3 w$ located at coordinate $(\mathbf{r}, \mathbf{w})$ at time t. For clarity we state that $\mathbf{r}$ represents the position and $\mathbf{w}$ the velocity. The reason we use this notation is in order to be able to use $\mathbf{v}$ for the fluid velocity below. Also, from now on we simply write $f_j(\mathbf{r}, \mathbf{w}, t) := f_j$, unless we want to write any dependency explicitly. With this definition of the distribution function we now define

$$\text{Particle density } n_j = \int f_j d\mathbf{w} \tag{2.1a}$$

$$\text{Fluid velocity } \mathbf{v}_j = \frac{1}{n_j}\int \mathbf{w} f_j d\mathbf{w} \tag{2.1b}$$

$$\text{Plasma pressure } p_j = \frac{m_j}{3}\int |\mathbf{w}-\mathbf{v}_j|^2 f_j d\mathbf{w} \tag{2.1c}$$

$$\text{Stress tensor } \pi_j = m_j \int (\mathbf{w}-\mathbf{v}_j)^2 f_j d\mathbf{w} - p_j \mathbf{I} \tag{2.1d}$$

$$\text{Heat flux } \mathbf{q}_j = \frac{m_j}{2}\int (\mathbf{w}-\mathbf{v}_j) \times |\mathbf{w}-\mathbf{v}_j|^2 f_j d\mathbf{w} \tag{2.1e}$$

The Vlasov equation

For a distribution function f_j it can be shown in the general case that the total derivative with respect to time to be equal to $C_j + S_j$, where C_j is the Coulomb collision operator and S_j is an external particle source. Written explicitely this becomes

$$\frac{df_j}{dt} = \frac{\partial f_j}{\partial t} + \frac{\partial f_j}{\partial x}\frac{\partial x}{\partial t} + \frac{\partial f_j}{\partial y}\frac{\partial y}{\partial t} + \frac{\partial f_j}{\partial z}\frac{\partial z}{\partial t} + \frac{\partial f_j}{\partial w_x}\frac{\partial w_x}{\partial t} + \frac{\partial f_j}{\partial w_y}\frac{\partial w_y}{\partial t} + \frac{\partial f_j}{\partial w_z}\frac{\partial w_z}{\partial t} = C_j + S_j \tag{2.2}$$

which can be written using more convenient notation as

$$\frac{\partial f_j}{\partial t} + \mathbf{w}\cdot\nabla f_j + \mathbf{a}\cdot\frac{\partial f_j}{\partial \mathbf{w}} = C_j + S_j \tag{2.3}$$

Using the Lorentz force equation given in equation 1.3 we can write $\mathbf{a} = \frac{\mathbf{F}}{m} = \frac{q}{m}(\mathbf{E} + \mathbf{w}\times\mathbf{B})$, giving us

$$\frac{\partial f_j}{\partial t} + \mathbf{w}\cdot\nabla f_j + \frac{q_j}{m_j}(\mathbf{E} + \mathbf{w}\times\mathbf{B})\cdot\frac{\partial f_j}{\partial \mathbf{w}} = C_j + S_j \tag{2.4}$$

This is the so called *Boltzmann equation.* We will assume that there are no particle sources or Coulomb collisions, thus $C_j = S_j = 0$, giving us the Vlasov equation

$$\frac{\partial f_j}{\partial t} + \mathbf{w}\cdot\nabla f_j + \frac{q_j}{m_j}(\mathbf{E} + \mathbf{w}\times\mathbf{B})\cdot\frac{\partial f_j}{\partial \mathbf{w}} = 0 \tag{2.5}$$

Moments of the Vlasov equation

By taking a moment of an equation we mean integrating the equation multiplied by w^n where n refers to the nth moment. We do this in order to lower the dimensionality of our equations from a dependency on $(\mathbf{r}, \mathbf{w}, t) \to (\mathbf{r}, t)$. As the zeroth, first and second moment of the Vlasov equation we get the following equations:

Continuity equation

$$\frac{\partial n_j}{\partial t} + \nabla \cdot (n_j \mathbf{v}_j) = 0 \tag{2.6}$$

Momentum balance equation

$$m_j n_j \frac{\partial \mathbf{v}_j}{\partial t} + m_j n_j \mathbf{v}_j \cdot \nabla \mathbf{v}_j = n_j q_j (\mathbf{E} + \mathbf{v}_j \times \mathbf{B}) - \nabla p_j - \nabla \cdot \pi_j \tag{2.7}$$

Energy equation

$$\frac{\partial}{\partial t}\left(\frac{1}{2} m_j n_j v_j^2 + \frac{3}{2} p_j\right) + \nabla \cdot \left[\left(\frac{1}{2} m_j n_j v_j^2 + \frac{5}{2} p_j\right)\mathbf{v}_j + \pi_j \cdot \mathbf{v}_j + \mathbf{q}\right] = \tag{2.8}$$

$$q_j n_j \mathbf{E} \cdot \mathbf{v}_j$$

where $\mathbf{E}$ and $\mathbf{B}$ are of course governed by Maxwells equations. The continuity equation simply states that the number of particles is conserved. The momentum balance equation can be interpreted as a fully written out version of Newton's second law $\mathbf{F} = m\mathbf{a}$, where the forces are gathered on the right hand side and accelerations on the left hand side. The energy equation describes the evolution of pressure in the plasma.

2.2 The Weiland fluid model

A model currently used in theoretical fusion plasma research at Chalmers is the Weiland model [5]. It is based on equations 2.6-2.8 for each plasma species $j = i, e$, for ions and electrons respectively. The equations are truncated by the diamagnetic heat flux in the energy equation. We will use this model henceforth assuming that the plasma only has one ion species present, and that it is an isotope of hydrogen.

In order to calculate the stability properties of the plasma, we assume equations 2.6-2.8 and that the particle density $n = n_0 + \delta n$ and the temperature $T = T_0 + \delta T$, where δn and δT are perturbations, which are Fourier decomposed as $\sim e^{i(\mathbf{k}\cdot\mathbf{r} - \omega t)}$, where $\mathbf{k} = (k_x, k_\perp, k_\parallel)$ and $\mathbf{r} = (x, y, z)$, as per the coordinate designation we introduced for a tokamak in chapter 1. It is assumed that $k_\parallel << k_\perp$ and that $\frac{\omega}{k_\parallel}$ is much larger than the thermal velocity for ions but much smaller than the thermal velocity of the electron.

As for ω, it is generally complex with $\omega = \omega_r + i\gamma$, with a $\gamma > 0$ generating an instability for quantity X as

$$\delta X \sim e^{i(\mathbf{k}\cdot\mathbf{r} - (\omega_r + i\gamma)t)} = e^{i(\mathbf{k}\cdot\mathbf{r} - \omega_r t)} e^{\gamma t} \tag{2.9}$$

which we see grows indefinitely with increasing t.

For the definitions of a plasma we assumed quasi-neutrality, which we will now also assume to the first order in the variations of n_i and n_e, i.e.

$$\delta n_i \approx \delta n_e \tag{2.10}$$

These assumptions, coupled with equation 2.6, 2.7 and 2.6 in the low frequency regime, provides the basis of the Weiland model.

In order to further investigate possible instabilities in the plasma the real frequency ω_r and the growth rate γ is needed. The assumption of quasi-neutrality leads to a dispersion relation[1], which is a fourth grade polynomial in ω, and thus has at most two roots with positive imaginary part that would lead to instabilities. These two modes are called the *Ion Temperature Gradient mode* and the *Trapped Electron mode*, or ITG mode and TEM for short. In certain parameter regions ($\hat{N}_i >> \hat{N}_e$ and $\hat{N}_e >> \hat{N}_i$) these modes become decoupled as can be described by two independent equations, which are derived in appendix A.

For the TE mode we have that the normalized growth rate $\hat{\gamma}$ is largely driven by the electron temperature gradient $\frac{R}{L_{T_e}}$ and the density gradient $\frac{R}{L_n}$, while the ITG mode is driven by the ion temperature gradient $\frac{R}{L_{T_i}}$ and the density gradient $\frac{R}{L_n}$ works to stabilize the growth rate.

These modes and their respective growth rates are very important to study as we have that the energy confinement time $\tau_E \propto \frac{1}{\gamma^3}$, so it is of great interest to see what drives these instabilities in order to be able to increase τ_E.

A major advantage that comes with the fluid equations is that results from this model are much more computationally efficient than more advanced fluid models, while still providing fairly good results when compared with experiments.

---

[1] Equation A.1 in appendix A

Chapter 3

Particle transport

In a fusion plasma there are various kinds of transport due to both classical collisions between particles but also due to the effects described in appendix C, collectively called anomalous transport. Most of the transport in a fusion plasma is due to this anomalous transport and in this chapter we will derive some equations describing the flux of particles with the starting point in known results from the Weiland model. We apply the Weiland model to two different problems, namely finding the flux of particles and finding the value of $\frac{R}{L_n}$ for which the flux is zero.

3.1 Particle flux

In general we have that the flux of particles in a fluid is given by

$$\Gamma_n =< \delta n \mathbf{v}_{E_r} >= -D\nabla n \tag{3.1}$$

i.e the flux is calculated as a spatial and temporal average of the product $\delta n \mathbf{v}_{E_r}$, where δn refers to the variation in particle density n and $\mathbf{v}_{E_r}$ is the radial electrostatic drift given by equation C.13. D is the effective particle diffusion coefficient and will be given for the Weiland model below. In a similar way the temperature flux is given by

$$\Gamma_{T_j} =< \delta T_j \mathbf{v}_{E_r} >= -\chi_j \nabla T_j \tag{3.2}$$

where δT_j is the pertubation of T_j. In this chapter we will focus on the transport of particles given by equation 3.1 but a similar treatment of the temperature transport can be found in appendix B.

According to [3],[5] we have, for the Weiland model, that

$$D = -\frac{\hat{\gamma}^3 \omega_{De}}{k_x^2} f_t \Delta_n \tag{3.3}$$

where

$$\Delta_n = \frac{1}{\hat{N}}\left[|\hat{\omega}^2|(\epsilon_n - 1) + \hat{\omega}_r\left(\frac{14}{3} - 2\eta_e - \frac{10}{3}\epsilon_n\right) + \frac{5}{3}\left(-\frac{11}{3} + 2\eta_e + \frac{7}{3}\epsilon_n\right)\right] \tag{3.4}$$

and k_x is the wave number in the x-direction, $\hat{\gamma}$ is the growth rate, $\hat{\omega}_r$ is the real frequency, $\hat{\omega} = \hat{\omega}_r + i\hat{\gamma}$, ω_{De} is the electron diamagnetic frequency, $\epsilon_n = \frac{2L_n}{L_B}$, $\eta_e = \frac{L_n}{L_{T_i}}$ and f_t is the fraction of trapped electrons.

Rearranging the terms in order to make the ϵ_n and η_e dependencies clearer we get

$$D = -\frac{\hat{\gamma}^3 \omega_{De}}{k_x^2} \frac{f_t}{\hat{N}} \left[(|\hat{\omega}|^2 - \frac{10}{3}\hat{\omega}_r + \frac{35}{9})\epsilon_n + (\frac{10}{3} - 2\hat{\omega}_r)\eta_e + \frac{14}{3}\hat{\omega}_r - |\hat{\omega}|^2 - \frac{55}{9} \right] \quad (3.5)$$

Combining equations 3.1 and 3.5 we get

$$\Gamma_n = \frac{\hat{\gamma}^3 \omega_{De}}{k_x^2} \frac{f_t}{\hat{N}} \left[(|\hat{\omega}|^2 - \frac{10}{3}\hat{\omega}_r + \frac{35}{9})\epsilon_n + (\frac{10}{3} - 2\hat{\omega}_r)\eta_e + \frac{14}{3}\hat{\omega}_r - |\hat{\omega}|^2 - \frac{55}{9} \right] \nabla n \quad (3.6)$$

and by writing with $\epsilon_n = 2\frac{L_n}{L_B}$ and $\eta_e = \frac{L_n}{L_{T_e}}$ explicitly we get

$$\Gamma_n = \frac{\hat{\gamma}^3 \omega_{De}}{k_x^2} \frac{f_t}{\hat{N}} \left[2(|\hat{\omega}|^2 - \frac{10}{3}\hat{\omega}_r + \frac{35}{9})\frac{L_n}{L_B} + (\frac{10}{3} - 2\hat{\omega}_r)\frac{L_n}{L_{T_e}} + \frac{14}{3}\hat{\omega}_r - |\hat{\omega}|^2 - \frac{55}{9} \right] \nabla n \quad (3.7)$$

Due to the geometry of the tokamak it can be shown using Ampere's law and assuming that $\mathbf{B} = B(r)\hat{r}$ that $L_B = R$, where R is the major radius of the tokamak. By multiplying equation 3.7 by $\frac{R}{n}$ and remembering that $L_n = -\frac{n}{\nabla n}$, it can be written as

$$\frac{R\Gamma_n}{n} = -\frac{\hat{\gamma}^3 \omega_{De}}{k_x^2} \frac{f_t}{\hat{N}} \left[2(|\hat{\omega}|^2 - \frac{10}{3}\hat{\omega}_r + \frac{35}{9}) + (\frac{10}{3} - 2\hat{\omega}_r)\frac{R}{L_{T_e}} + (\frac{14}{3}\hat{\omega}_r - |\hat{\omega}|^2 - \frac{55}{9})\frac{R}{L_n} \right] \quad (3.8)$$

The first term inside the bracket is proportional to ∇B on the non-normalized form. The term will be positive for all values of $\hat{\omega}$ and thus always lead to an inward contribution of the particle flux, which is called a pinch. For the range of $\hat{\omega}_r$ and $\hat{\gamma}$ in the regions we are interested in, $\frac{R}{L_n}$ will contribute to a positive flux and thus be diffusive, while $\frac{R}{L_{T_e}}$ will have a negative contribution. However, since both $\hat{\omega}_r$ and $\hat{\gamma}$ are dependent on both $\frac{R}{L_n}$ and $\frac{R}{L_{T_e}}$, we will need to conduct simulations in order to better determine where the flux is positive or negative, as well as where each mode is dominant.

3.2 The peaking factor

We are interested in finding for which density gradient the total flux is equal to zero. This is the density gradient we expect to find in a steady state plasma core where there are no particle sources. This value of the density gradient is called the *peaking factor*

$$\mathrm{PF} = \left. \frac{R}{L_n} \right|_{\Gamma_n = 0} \quad (3.9)$$

When the peaking factor is positive it means that the density profile is peaked, corresponding to an inward pinch. Conversely, a negative peaking factor would result from an outward pinch flux. For particles serving as fuel for

the fusion reaction a positive peaking factor is desired, while negative peaking factors for impurities would be greatly beneficial.
For the flux given by equation 3.8. we simply note that for the flux to be zero we have that the terms in the brackets must add to zero. Some rearranging of the terms yields

$$\left.\frac{R}{L_n}\right|_{\Gamma_n=0} = \frac{2\big(|\hat{\omega}|^2 - \frac{10}{3}\hat{\omega}_r + \frac{35}{9}\big) + \frac{R}{L_{T_e}}\big(\frac{10}{3} - 2\hat{\omega}_r\big)}{|\hat{\omega}|^2 + \frac{55}{9} - \frac{14}{3}\hat{\omega}_r} \tag{3.10}$$

Peaking factors for various $\hat{\omega}_r$ and $\hat{\gamma}$

If we assume that we are close to marginal stability so that $\hat{\gamma} << \hat{\omega}_r \Rightarrow \hat{\omega} \approx \hat{\omega}_r$, we get the general expression

$$\left.\frac{R}{L_n}\right|_{\hat{\omega}_r>>\hat{\gamma}} = \frac{2(\hat{\omega}_r^2 - \frac{10}{3}\hat{\omega}_r + \frac{35}{9}) + \frac{R}{L_{T_e}}(\frac{10}{3} - 2\hat{\omega}_r)}{\hat{\omega}_r^2 - \frac{14}{3}\hat{\omega}_r + \frac{55}{9}} \tag{3.11}$$

and similarly far away from marginal stability we have $\hat{\gamma} >> \hat{\omega}_r$

$$\left.\frac{R}{L_n}\right|_{\hat{\gamma}>>\hat{\omega}_r} = \frac{2(\hat{\gamma}^2 + \frac{35}{9}) + \frac{10R}{3L_{T_e}}}{\hat{\gamma}^2 + \frac{55}{9}} \tag{3.12}$$

We take a closer look at the case when the real part of $\hat{\omega}$ is dominant. As shown in appendix A the real parts of the TE and ITG modes can be written approximately as

$$\hat{\omega}_r^{TEM} = \frac{10g}{3} - \frac{1}{2}\frac{f_t}{1-f_t}\left(\frac{1}{\epsilon_n} - g\right) \tag{3.13}$$

and

$$\hat{\omega}_r^{ITG} = \frac{3\tau + (10f_t - 10 - 3\tau)\epsilon_n}{6\tau(1-f_t)\epsilon_n} \tag{3.14}$$

respectively. Using these equations we can get a complete analytical equation for the peaking factors in these cases. For the case when the TE mode dominates we get

$$\left.\frac{R}{L_n}\right|_{\hat{\omega}_r>>\hat{\gamma}}^{TEM} = \frac{\frac{100}{36}g^2 - \frac{10}{6}g\kappa + \frac{\kappa^2}{4} - \frac{50}{9}g + \frac{5}{3}\kappa + \frac{35}{9} + \frac{R}{L_{T_e}}\big(\frac{10}{3}(1-\frac{g}{2}) + \kappa\big)}{\frac{100}{36}g^2 - \frac{10}{6}g\kappa + \frac{\kappa^2}{4} - \frac{70}{9}g + \frac{7}{3}\kappa + \frac{55}{9}} \tag{3.15}$$

where

$$\kappa = \frac{f_t}{1-f_t}\left(\frac{1}{\epsilon_n} - g\right) = \frac{f_t}{1-f_t}\left(2\frac{R}{L_n} - g\right) \tag{3.16}$$

As for the ITG mode dominated case we get

$$\left.\frac{R}{L_n}\right|_{\hat{\omega}_r>>\hat{\gamma}}^{ITG} = \frac{\alpha + \beta\frac{R}{L_{T_e}}}{\zeta} \tag{3.17}$$

where

$$\begin{aligned}\alpha = 18\tau^2\epsilon_n^2 - 36\tau^2\epsilon_n + 18\tau^2 + 120\epsilon_n^2\tau(1-f_t) - 120\tau\epsilon_n(1-f_t) + 200\epsilon_n^2(1-f_t)^2 \\ -120\tau^2\epsilon_n(1-f_t) + 400\tau\epsilon_n(1-f_t) + 120\tau^2\epsilon_n(1-f_t) + 280\tau^2\epsilon_n^2(1-f_t)^2\end{aligned} \tag{3.18}$$

$$\beta = 120\tau^2\epsilon_n^2(1-f_t)^2 - 36\tau^2\epsilon_n(1-f_t) + 60\tau\epsilon^2(1-f_t)^2 + 18\tau^2\epsilon^2(1-f_t) \tag{3.19}$$

$$\begin{aligned}\zeta = 9\tau^2\epsilon_n^2 - 18\tau^2\epsilon_n + 9\tau^2 + 60\epsilon_n^2\tau(1-f_t) - 60\tau\epsilon_n(1-f_t) + 100\epsilon_n^2(1-f_t)^2 \\ -84\tau^2\epsilon_n(1-f_t) + 280\tau\epsilon_n^2(1-f_t)^2 + 84\tau^2\epsilon_n(1-f_t) + 220\tau^2\epsilon_n^2(1-f_t)^2\end{aligned} \tag{3.20}$$

As can be seen the expressions for the peaking factors become rather cumbersome even in simple cases. A further complication comes from the fact that in both cases we have $\frac{R}{L_n}$ on both sides of the equations since $\epsilon_n = 2\frac{L_n}{L_B} = 2\frac{L_n}{R} = 2\frac{1}{R/L_n}$ so finding an expression for the peaking factor analytically becomes quite cumbersome, especially when we allow for larger $\hat{\gamma}$. So when we look for the peaking factor in these complicated cases we simply find $\frac{R}{L_n}$ for which equation 3.8 equals to zero. This will be shown in more detail in chapter 4.

3.3 Pellet fueling application

A possible application for the results above is a new method of adding additional fuel to an ignited fusion plasma called *pellet fueling*. It is desirable to find a more efficient fueling method than the currently used hydrogen gas infusion and pellet fueling is a candidate for such a method. The main idea is to shoot frozen pellets of deuterium and tritium into the plasma in order to add more fuel for the fusion process. However, due to the turbulent nature of the plasma only some parts of the fuel will be absorbed and given a chance to participate in the fusion process while the rest will be forced out of the plasma as part of the diffusion. A projected additional benefit from pellet fueling is that it can be used as a method to control spontaneous instabilities at the edge of the plasma, which would reduce the long term strain on the walls of the reactor. For our purposes we are very interested in the flux of particles for negative $\frac{R}{L_n}$, as this will indicate whether parts of the pellet will be sucked into the plasma core or not.

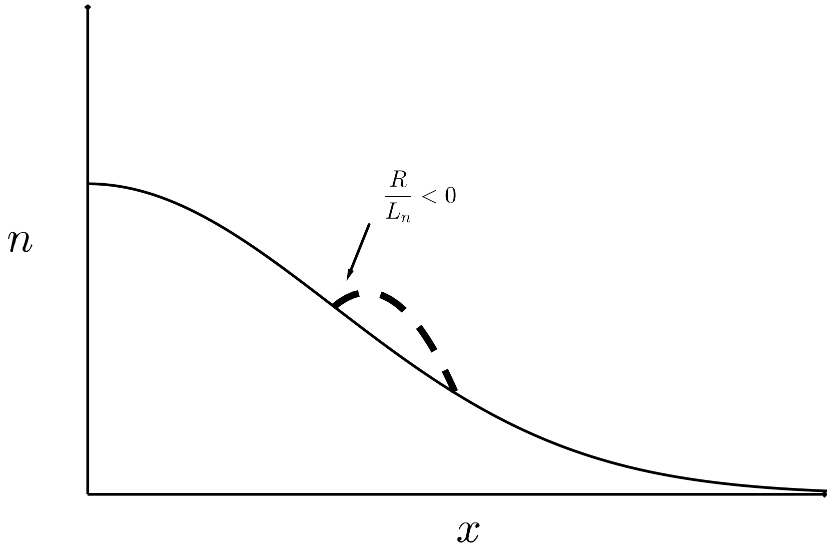

Figure 3.1: Exaggerated particle density for the plasma after being hit by a pellet.

Chapter 4

Simulations

In order to better visualize the behavior and nature of the flux of particles resulting from the assumptions made in the approximate version of the Weiland model used here we will investigate the particle flux and peaking factor and their dependencies on plasma parameters such as various gradients and values of $k_\perp \rho$, as well as investigate how the different modes are influenced and where each of them dominates. The simulations were done in Matlab where the values of the various quantities depending on $\frac{R}{L_n}$ were stored in a vector and then plotted accordingly for different values of $\frac{R}{L_{T_i}}$ and $\frac{R}{L_{T_e}}$ in order to determine the dependency on them as well.

4.1 Particle flux in pellet fueled plasmas

We wish take a better look at the behavior of equation 3.8 as a function of $\frac{R}{L_n}$. In order to make the simulations more straightforward we multiply the equation with[1] $\frac{k_x^2}{\omega_{De}}$ and get

$$\frac{k_x^2}{\omega_{De}} \frac{R\Gamma_n}{n} = -\hat{\gamma}^3 \frac{f_t}{\hat{N}} \left[2(|\hat{\omega}|^2 - \frac{10}{3}\hat{\omega}_r + \frac{35}{9}) + (\frac{10}{3} - 2\hat{\omega}_r)\frac{R}{L_{Te}} + (\frac{14}{3}\hat{\omega}_r - |\hat{\omega}|^2 - \frac{55}{9})\frac{R}{L_n} \right] \tag{4.1}$$

We can see that $\Gamma_n \propto \hat{\gamma}^3$, so the flux is driven by instabilities in the ITG and TE mode and the flux is equal to zero when $\hat{\gamma} = 0$.

We note that the $\frac{R}{L_{Te}}$ term will give a positive contribution to the flux for $\hat{\omega}_r > \frac{10}{6}$ and a negative one otherwise. The $\frac{R}{L_{Ti}}$ dependency only comes in through $\hat{\omega}_r$ and $\hat{\gamma}$ for the the ITG mode.

The values used for the simulations are $\tau = 1$, $f_t = 0.5$ and $k_\perp \rho = 0.2$, corresponding to typical tokamak parameters used in simulations. In order to get realistic results we use the $\hat{\omega}_r$ and $\hat{\gamma}$ expressions for the ITG and TE modes derived in appendix A, which are also written here for convenience.

---

[1] This does not alter the form of the graph as k_x^2 is a positive number and $\omega_{De} = 2\frac{k_\perp T_e}{qB}\frac{\nabla B}{B} = 2\frac{k_\perp T_e}{|q|BR}$, which is also always positive. As we are mainly interested in where the flux is positive, negative or zero, we get the same information by looking at the graph for this equation.

ITG mode frequency and growth rate

As is shown in appendix A, the solution to the dispersion relation $\hat{\omega}(k)$ is given by

$$\hat{\omega}_r = \frac{3\tau + (10f_t - 10 - 3\tau)\epsilon_n}{6\tau(1-f_t)\epsilon_n} + \frac{k_\perp^2\rho^2}{2\epsilon_n\tau(1-f_t)}\left[(\frac{5}{3} + \frac{\tau}{1-f_t})\epsilon_n - \eta_i - 1 - \frac{\tau}{1-f_t}\right] \tag{4.2}$$

and

$$\hat{\gamma} = \sqrt{\frac{\eta_i - \eta_{ith}}{\tau\epsilon_n(1-f_t)}}\left[1 - \frac{k_\perp^2\rho^2}{1-f_t}\left(1 - \frac{(1+\epsilon_n)}{4\epsilon_n}\right)\right] \tag{4.3}$$

where

$$\begin{aligned}\eta_{ith} \approx \frac{2}{3} + \frac{\tau}{2(1-f_t)}\left(\frac{1}{2\epsilon_n} - 1\right) + \left(\frac{10(1-f_t)}{9\tau} + \frac{\tau}{4(1-f_t)}\right)\epsilon_n + \\ \frac{k_\perp^2\rho^2}{\tau}\left[-\frac{\tau^2}{8(1-f_t)^2\epsilon_n^2} + \frac{\tau}{1-f_t}\left(\frac{\tau}{8(1-f_t)} - \frac{5}{6}\right)\frac{1}{\epsilon_n} + \frac{5\tau}{3(1-f_t)} - \frac{5}{9} + \right. \\ \left. \frac{\tau^2}{8(1-f_t)^2} + \left(\frac{5}{9} - \frac{5\tau}{6(1-f_t)} - \frac{\tau^2}{8(1-f_t)^2}\right)\epsilon_n\right]\end{aligned} \tag{4.4}$$

TE mode frequency and growthrate

For the TEM mode we use the same values as for the ITG mode and in addition put the shear factor $g = 1$.

$$\hat{\omega}_r = \frac{10g}{6} - \frac{1}{2}\frac{f_t}{1-f_t}\left(\frac{1}{\epsilon_n} - g\right) \tag{4.5}$$

and

$$\hat{\gamma} = \sqrt{\frac{f_t(\eta_e - \eta_{eth})}{\epsilon_n(1-f_t)}} \tag{4.6}$$

where

$$\eta_{eth} = \frac{2}{3} - \frac{f_t}{2(1-f_t)} + \frac{10\epsilon_n g(1-f_t)}{9f_t} + \frac{f_t\epsilon_n g}{4(1-f_t)} + \frac{f_t}{4\epsilon_n g(1-f_t)} \tag{4.7}$$

Note that the TE mode has neither a η_i nor a $k_\perp\rho$ dependency.

We plot the flux stemming from each mode as well as the different modes respective $\hat{\omega}_r$ and $\hat{\gamma}$ in order to be able to determine their effect on the flux as a whole.

In order to keep track of when our approximations are valid we also plot $\hat{N}_i/\hat{N}_e$ to indicate that the TE mode approximation is valid when $\hat{N}_i/\hat{N}_e << 1$ and the ITG mode approximation when $\hat{N}_i/\hat{N}_e >> 1$, as these assumptions were made when deriving the expression for the respective modes. We can also tell which mode is dominant by looking at which has the largest growth rate, and we find that both these methods agree with each other for all conducted simulations. ITG plots are in red, TEM in blue.

We start out by looking at the case when $\frac{R}{L_{T_e}} << \frac{R}{L_{T_i}}$, and thus the ITG mode,driven by $\frac{R}{L_{T_i}}$, dominates. As we can see in figure 4.1 the ITG flux dominates, but we can only rely on these results in the region where $\hat{N}_i >> \hat{N}_e$, which as can be seen in the top right corner is where $\frac{R}{L_n}$ is approximately smaller than 5. In this region the flux goes from being negative to being positive. As for the $\hat{\omega}_r$ for each mode, we see that they are virtually linearly dependent on $\frac{R}{L_n}$ with $\hat{\omega}_{\text{ITG}} < 0$ and $\hat{\omega}_{\text{TE}} > 0$ for $\frac{R}{L_n} \lesssim 5$, while the growth rate $\hat{\gamma}$ instead has a maximum value and will always be positive, as can be expected from equations 4.3 and 4.6, as long as f_t is not extremely large.

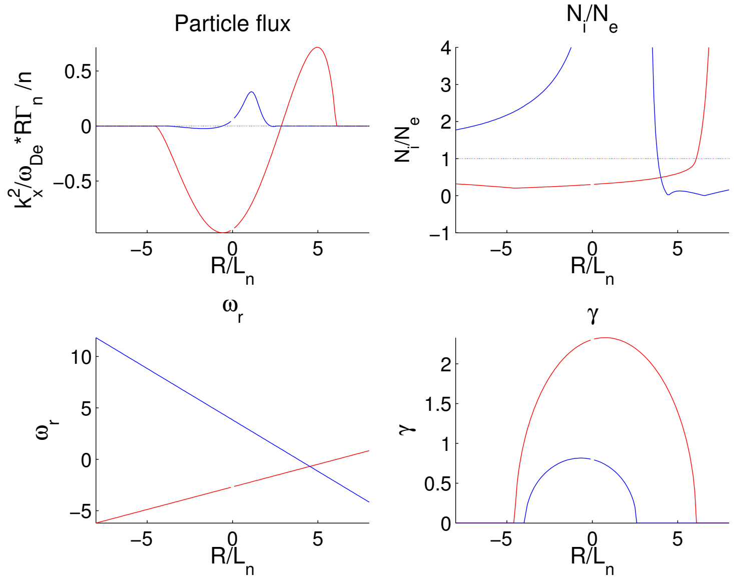

Figure 4.1: $\frac{R}{L_{T_i}} = 8$, $\frac{R}{L_{T_e}} = 4$

We see that the peaking factor for the ITG flux is 2.2 and that the flux is negative for smaller value and positive for larger values. The fact that the flux is negative for negative $\frac{R}{L_n}$ is beneficial to the proposed concept of pellet fueling as the application would only work given such an inward flux toward the plasma core. For $\frac{R}{L_n} = 0$ we have a negative flux for the ITG mode and a positive flux for the TE mode. In the next section we will show additional fluxes for more values of $\frac{R}{L_{T_i}}$ and $\frac{R}{L_{T_e}}$ in the context of evaluating the factors that affect the peaking factors.

For the TEM dominated case we see in figure 4.2 that $\hat{N}_i << \hat{N}_e$ for all $\frac{R}{L_n}$, meaning that our approximations should yield an accurate flux overall. We note that the shape of the flux graph resembles a mirrored version of the ITG flux in figure 4.1. The TEM dominated flux appears to have multiple zeroes, but it is likely that except for the zero at $\frac{R}{L_n} = 2.2$, they do not actually represent a real peaking factor but is due to numerical approximations.

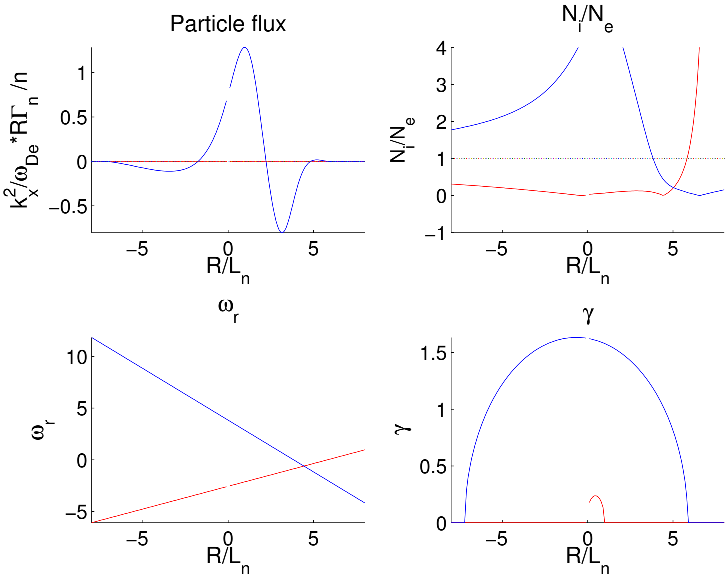

Figure 4.2: $\frac{R}{L_{T_i}} = 2$, $\frac{R}{L_{T_e}} = 8$

In contrast to the ITG mode, the TE mode has a positive flux for negative $\frac{R}{L_n}$ indicating that pellet fueling would not work well for this mode, which would result in the injected fuel being transported toward the plasma edge region.

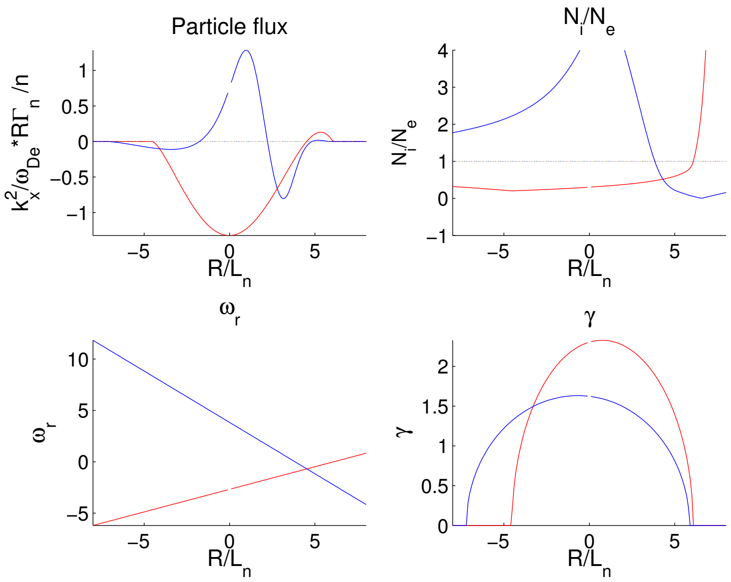

Figure 4.3: $\frac{R}{L_{T_i}} = 8$, $\frac{R}{L_{T_e}} = 8$

When looking at the case when both modes contribute to the flux, as seen in figure 4.3, we can see that the ITG flux is mostly negative and the TEM flux mostly positive. This region for which the validity of the approximations become uncertain exists for other values of $\frac{R}{L_{T_e}}$ and $\frac{R}{L_{T_i}}$ as well and additional figures with more of these values are found in appendix D. As in the dominated cases the ITG and TE mode are symmetrical which underlines the fact that pellet fueling would only work for the ITG mode.

4.2 Peaking factors

As we saw in chapter 3, it is difficult to express the peaking factor PF $= \frac{R}{L_n}\big|_{\Gamma_n=0}$ analytically so we will simply get the peaking factor by plotting the flux given by equation 4.1 and find the value for when $\Gamma_n = 0$ numerically. Since we know from the previous section where each mode dominates, we pick suitable values of $\frac{R}{L_{T_e}}$ and $\frac{R}{L_{T_i}}$ in order to ensure that the mode we investigate is dominant in the relevant region. We start out by investigating the behavior of the ITG mode for various $\frac{R}{L_{T_e}}$ and $k_\perp\rho$.

ITG mode dominated plasmas

In figure 4.8 we have plotted the ITG mode flux for $\frac{R}{L_{T_i}} = 8$, insuring that we have overall ITG dominance, and set $\frac{R}{L_{T_e}}$ to 2,4,6 and 8. From the figure we can see that as far as the peaking factor goes, it increases for larger values of $\frac{R}{L_{T_e}}$, consistent with the observation of a negative contribution to the flux from $\frac{R}{L_{T_e}}$ in equation 4.1. The numerical values for the resulting peaking factors are given in table 4.1, where we see that $\hat{\omega}_r$ increases with $\frac{R}{L_{T_e}}$, while $\hat{\gamma}$ decreases.

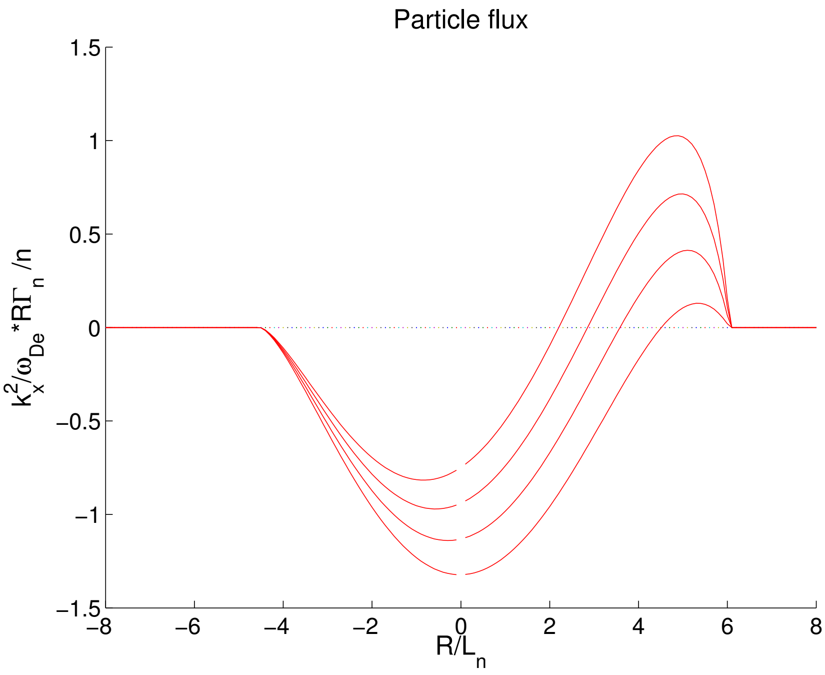

Figure 4.4: The ITG driven particle flux with $\frac{R}{L_{Te}}$ as a parameter. The graph is shifted to the right with increasing $\frac{R}{L_{Te}}$.

$\frac{R}{L_{Te}}$	PF	$\hat{\omega}_r$	$\hat{\gamma}$
2	2.2	-1.7120	2.2394
4	2.9	-1.4040	2.1274
6	3.6	-1.0960	1.9621
8	4.5	-0.7000	1.64463

Table 4.1: Peaking factors for the ITG mode.

Varying $k_\perp\rho$ shows that while the flux is somewhat altered, the peaking factors stay virtually the same. Looking at equation 4.1, 4.2 and 4.3 we that $\hat{\gamma}^3$ is a multiplicative factor so any small change in $\hat{\gamma}$ will alter the amplitude of Γ_n, but the zeros of equation 4.1 remain largely the same. We note that for $k_\perp\rho = 0.4$, the flux goes to infinity for large $\frac{R}{L_n}$. This is a result a breakdown of the approximation $k_\perp^2\rho^2 << 1$ used to derive equations 4.2 and 4.3. Because of this, the η_{ith} term will never cancel out the η_i term in equation 4.3.

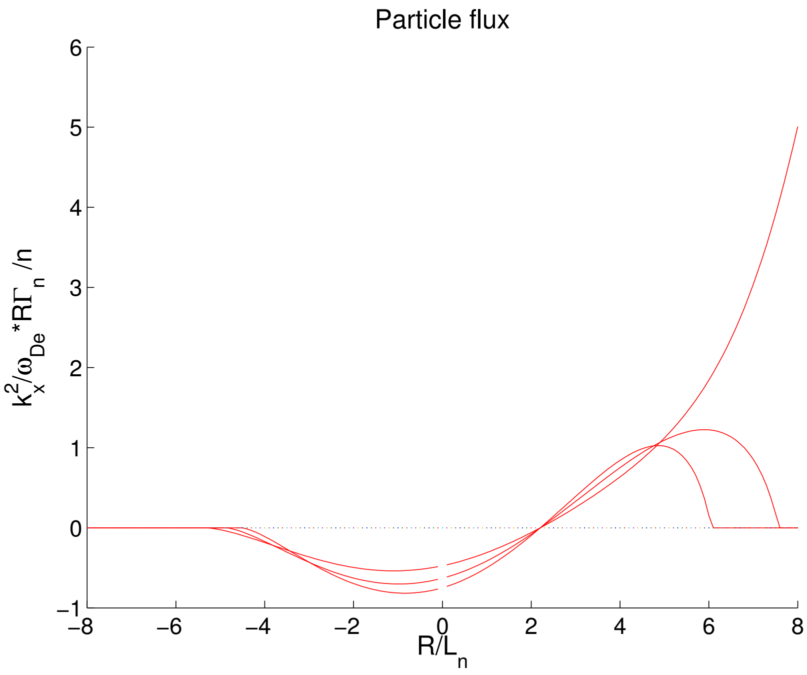

Figure 4.5: The ITG driven flux with $k_\perp\rho$ as a parameter. The amplitude of the flux increases with growing $k_\perp\rho$.

$k_\perp\rho$	PF	$\hat{\omega}_r$	$\hat{\gamma}$
0.2	2.2	-1.7120	2.2394
0.3	2.2	-1.8937	2.1304
0.4	2.2	-2.1480	1.9776

Table 4.2: Peaking factors for the ITG mode for various $k_\perp\rho$

TE mode dominated case

Since the TE mode does not have any $k_\perp\rho$ dependency under the present approximations, we will only investigate how the peaking factor relates to $\frac{R}{L_{T_e}}$. We see that $\hat{\omega}_r$ is unaffected by changes in $\frac{R}{L_{T_e}}$ so the zeros of the flux, and thus peaking factors remain unaltered by varying $\frac{R}{L_{T_e}}$. This is due to a cancellation of the factor $\frac{10}{3} - 2\hat{\omega}_r$ in the term containing the $\frac{R}{L_{T_e}}$ factor in equation 4.1. We do however get larger variation in $\hat{\gamma}$, but this only serves to increase the amplitude of the flux and has no major effect on the peaking factors.

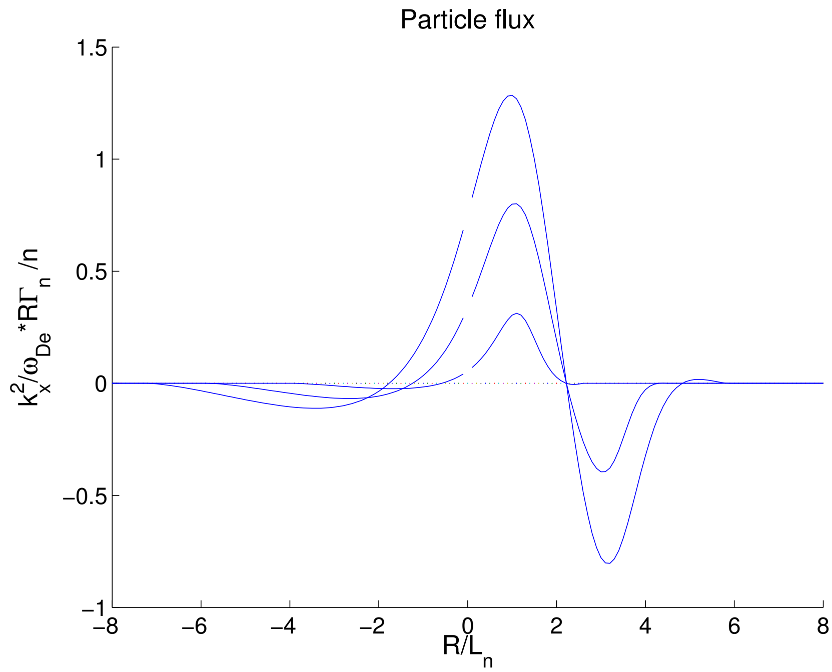

Figure 4.6: The TEM driven flux with $\frac{R}{L_{T_e}}$ as a parameter. In this graph the amplitude of the flux increases with growing $\frac{R}{L_{T_e}}$.

$\frac{R}{L_{T_e}}$	PF	$\hat{\omega}_r$	$\hat{\gamma}$
4	2.3	1.5333	0.3415
6	2.3	1.5333	1.0567
8	2.3	1.5333	1.4549

Table 4.3: Peaking factors for the TE mode for various $\frac{R}{L_{T_e}}$ for $\frac{R}{L_{T_i}} = 2$.

We note that for the TE mode dominated plasmas the peaking factors are usually smaller that for ITG mode plasmas.

Summary and conclusions

In this thesis we have tried to get a deeper insight into what drives the turbulent transport of the fusion plasma contained in a tokamak. Starting with the Weiland model and some known results, an analytical treatment of the flux of particles and heat[2] resulted in expressions for the normalized flux and how it depends on parameters such as temperature and particle density gradients. For cases when the eigenvalues $\hat{\omega}$ does not depend on the density gradient we could even get an accurate expression for the peaking factor for the particle density.

In order to better visualize the results, simulations of the flux were made using realistic values of $\hat{\omega}_r$ and $\hat{\gamma}$ for both ITG and TE mode dominated plasmas. From these simulations it was also possible to obtain the peaking factors and their dependency on gradients and $k_\perp \rho$. It turned out that, overall, the dependency on these parameters were rather weak for the parameters used in the simulations.

When it comes to the possible application of pellet fueling it was found that a negative density gradient would yield an inward particle flux for the ITG mode but not for the TE mode. This means that for a ITG mode dominated plasma it would be possible to insert additional fuel into the plasma core by the method of pellet fueling.

Possible future work

In order to see how accurate the flux derived analytically from the fluid equations of the Weiland model are, further study and comparison with more advanced models can be done. For example, the simulations should be done for more values of τ, f_t, g and so on. If gyrokinetic simulations were carried out they could be compared to the results in this thesis in order to determine their accuracy, and if so, could possible indicate any advantages that comes from using a computationally efficient fluid model. If the differences between the fluid simulations and gyrokinetic simulations are minor, using the fluid equations could save computing time for simulations in certain regimes. Ultimately though, the results must be compared to experiments, which would determine their accuracy and eventual usefulness.

---

[2] See appendix B

Bibliography

[1] Jeffrey Friedberg (2012), *Plasma physics and fusion energy*, Massachusetts Institute of Technology, Cambridge.

[2] Dan Andersson, Mietek Lisak, Pontus Johannisson, Mattias Marklund (2003), *Basic Plasma Physics, Theory and applications*, Department of Electromagnetics, Chalmers University of Technology, Gothenburg.

[3] Giovanni Tardini (2003), *Validation of theory based transport models in tokamak plasmas*, Max-Planck-Institut für Plasmaphysik, Munich.

[4] Jan Weiland (2012), *Stability and transport on magnetic confinement systems*, Chalmers University of Technology, Gothenburg.

[5] Jan Weiland (1999), *Collective modes in inhomogenous plasmas*, Chalmers University of Technology, Gothenburg.

[6] Andreas Skyman (2014), *Gyrokinetic simulations of turbulent transport in tokamak plasmas*, Chalmers University of Technology, Gothenburg.

[7] Daniel Tegnered (2015), *Gyrokinetic simulations of turbulent particle and heat transport in tokamaks*, Chalmers University of Technology, Gothenburg.

[8] A. Heikkilä and J. Weiland (1993), *Transport dure to ion-temperature-gradient-driven magnetic modes*, Chalmers University of Technology, Gothenburg.

[9] A. Skyman, D. Tegnered, H. Nordman, P. Strand (2014), *Gyrokinetic modelling of stationary electron and impurity profiles in tokamaks*, Chalmers University of Technology, Gothenburg.

[10] J. Andersson, H. Nordman, R. Singh, J. Weiland (2006), *Zonal flow generation in collisioness trapped electron mode turbulence*, Chalmers University of Technology, Gothenburg.

Appendix A

Derivations

Finding $\hat{\omega} = \hat{\omega}_r + i\hat{\gamma}$ from quasi-neutrality

We start by assuming quasi-neutrality and writing the fraction of trapped electrons as f_t, which can, according to [3], be written as

$$\hat{N}_i \hat{N}_e \epsilon_n \frac{T_e}{e\phi}\left[\frac{\delta n_i}{n_i} - f_t \frac{\delta n_{et}}{n_{et}} - (1-f_t)\frac{\delta n_{ep}}{n_{ep}}\right] = 0 \tag{A.1}$$

Assuming that the passing electrons are adiabatic we have

$$\frac{\delta n_{ep}}{n_{ep}} = \frac{e\phi}{T_e} \tag{A.2}$$

In [3], it is shown that

$$\frac{\delta n_{et}}{n_{et}} = \frac{e\phi}{T_e}\frac{1}{\hat{N}_e}\frac{1}{\epsilon_n}\left[\hat{\omega}(1-\epsilon_n) + \eta_e + \frac{5}{3}\epsilon_n - \frac{7}{3}\right] \tag{A.3}$$

and

$$\begin{aligned}\frac{\delta n_i}{n_i} = \frac{e\phi}{T_e}\frac{1}{\hat{N}_i}\frac{1}{\epsilon_n}\hat{\omega}_{De}^2\Bigg[& -\hat{\omega}^2 k_\perp^2 \rho^2 \epsilon_n + \hat{\omega}\left(1 - \epsilon_n - \frac{5}{3}k_\perp^2\rho^2\frac{\epsilon_n}{\tau} - k_\perp^2\rho^2\frac{1+\eta_i}{\tau}\right) \\ & -\frac{1}{\tau}\left(\eta_i - \frac{7}{3} + \frac{5}{3}\epsilon_n\right) - k^2\rho^2\frac{5}{3\tau^2}(1+\eta_i)\Bigg]\end{aligned} \tag{A.4}$$

Inserting equation A.2, A.3 and A.4 into A.1 gives

$$\begin{aligned}\hat{N}_e\Bigg[& -\hat{\omega}^2 k^2\rho^2\epsilon_n + \hat{\omega}\left(1 - \epsilon_n - k_\perp^2\rho^2\frac{5\epsilon_n}{3\tau} - k_\perp^2\rho^2\frac{1+\eta_i}{\tau}\right) \\ & -\frac{1}{\tau}\left(\eta_i - \frac{7}{3} + \frac{5}{3}\epsilon_n\right) - k_\perp^2\rho^2\frac{5}{3\tau^2}(1+\eta_i)\Bigg] = \\ & = (1-f_t)\hat{N}_i\hat{N}_e\epsilon_n + f_t\hat{N}_i\left[\hat{\omega}(1-\epsilon_n) + \left(\eta_e - \frac{7}{3} + \frac{5}{3}\epsilon_n\right)\right]\end{aligned} \tag{A.5}$$

Dividing this equation with $\hat{N}_i\hat{N}_e$ gives

$$\frac{1}{\hat{N}_i}\Bigg[-\hat{\omega}^2k_\perp^2\rho^2\epsilon_n+\hat{\omega}\left(1-\epsilon_n-k_\perp^2\rho^2\frac{5\epsilon_n}{3\tau}-k_\perp^2\rho^2\frac{1+\eta_i}{\tau}\right)$$

$$-\frac{1}{\tau}\left(\eta_i-\frac{7}{3}+\frac{5}{3}\epsilon_n\right)-k_\perp^2\rho^2\frac{5}{3\tau^2}(1+\eta_i)\Bigg]=$$

$$=(1-f_t)\epsilon_n+\frac{f_t}{\hat{N}_e}\left[\hat{\omega}(1-\epsilon_n)+\left(\eta_e-\frac{7}{3}+\frac{5}{3}\epsilon_n\right)\right] \tag{A.6}$$

The ITG mode

For $\hat{N}_i << \hat{N}_e$ equation A.6 can be reduced to

$$\Bigg[-\hat{\omega}^2k_\perp^2\rho^2\epsilon_n+\hat{\omega}\left(1-\epsilon_n-k_\perp^2\rho^2\frac{5\epsilon_n}{3\tau}-k_\perp^2\rho^2\frac{1+\eta_i}{\tau}\right)$$

$$-\frac{1}{\tau}\left(\eta_i-\frac{7}{3}+\frac{5}{3}\epsilon_n\right)-k_\perp^2\rho^2\frac{5}{3\tau^2}(1+\eta_i)\Bigg]=\hat{N}_i(1-f_t)\epsilon_n \tag{A.7}$$

With $\hat{N}_i=\hat{\omega}^2+\frac{10}{3\tau}\hat{\omega}+\frac{5}{3\tau^2}$ we can write the equation on the form

$$\hat{\omega}^2(1-f_t+k_\perp^2\rho^2)\epsilon_n+\hat{\omega}\left[\frac{10}{3\tau}(1-f_t)\epsilon_n+\epsilon_n+k_\perp^2\rho^2\frac{5}{3\tau}\epsilon_n+k_\perp^2\rho^2\frac{1+\eta_i}{\eta}-1\right]$$

$$+\left[\frac{5}{3\tau^2}(1-f_t)\epsilon_n+\frac{1}{\tau}\left(\eta_i+\frac{5}{3}\epsilon_n-\frac{7}{3}\right)+k_\perp^2\rho^2\frac{5}{3\tau^2}(1+\eta_i)\right]=0 \tag{A.8}$$

This is a second degree polynomial in $\hat{\omega}$, which can be written as

$$\hat{\omega}^2+A\hat{\omega}+B=0 \tag{A.9}$$

where

$$A=\frac{\frac{10}{3\tau}(1-f_t)\epsilon_n+\epsilon_n+k_\perp^2\rho^2\frac{5}{3\tau}\epsilon_n+k_\perp^2\rho^2\frac{1+\eta_i}{\eta}-1}{(1-f_t+k_\perp^2\rho^2)\epsilon_n} \tag{A.10}$$

and

$$B=\frac{\frac{5}{3\tau^2}(1-f_t)\epsilon_n+\frac{1}{\tau}(\eta_i+\frac{5}{3}\epsilon_n-\frac{7}{3})+k_\perp^2\rho^2\frac{5}{3\tau^2}(1+\eta_i)}{(1-f_t+k_\perp^2\rho^2)\epsilon_n} \tag{A.11}$$

Thus a general solution is given by

$$\hat{\omega}=\frac{A}{2}\pm\sqrt{\frac{A^2}{4}-B} \tag{A.12}$$

and we see that we have an imaginary part $\hat{\gamma}$ only if $\frac{A^2}{4}<B$. Performing a Taylor expansion to the first order in $k^2\rho^2$ gives

$$\hat{\omega}_r = \frac{3\tau + (10f_t - 10 - 3\tau)\epsilon_n}{6\tau(1-f_t)\epsilon_n} + \frac{k^2\rho^2}{2\epsilon_n\tau(1-f_t)}\left[(\frac{5}{3} + \frac{\tau}{1-f_t})\epsilon_n - \eta_i - 1 - \frac{\tau}{1-f_t}\right] \tag{A.13}$$

$$\hat{\gamma} = \sqrt{\frac{\eta_i - \eta_{ith}}{\tau\epsilon_n(1-f_t)}}\left[1 - \frac{k_\perp^2\rho^2}{1-f_t}\left(1 - \frac{(1+\epsilon_n)}{4\epsilon_n}\right)\right] \tag{A.14}$$

where

$$\eta_{ith} \approx \frac{2}{3} + \frac{\tau}{2(1-f_t)}\left(\frac{1}{2\epsilon_n} - 1\right) + \left(\frac{10(1-f_t)}{9\tau} + \frac{\tau}{4(1-f_t)}\right)\epsilon_n +$$

$$\frac{k_\perp^2\rho^2}{\tau}\left[-\frac{\tau^2}{8(1-f_t)^2\epsilon_n^2} + \frac{\tau}{1-f_t}\left(\frac{\tau}{8(1-f_t)} - \frac{5}{6}\right)\frac{1}{\epsilon_n} + \frac{5\tau}{3(1-f_t)} - \frac{5}{9} + \right.$$

$$\left.\frac{\tau^2}{8(1-f_t)^2} + \left(\frac{5}{9} - \frac{5\tau}{6(1-f_t)} - \frac{\tau^2}{8(1-f_t)^2}\right)\epsilon_n\right] \tag{A.15}$$

according to [8].

The TE mode

A similar treatment of equation A.6 while assuming that $\hat{N}_i << \hat{N}_e$ gives

$$\hat{N}_e(1-f_t)\epsilon_n + f_t\left[\hat{\omega}(1-\epsilon_n) + \left(\eta_e - \frac{7}{3} + \frac{5}{3}\epsilon_n\right) = 0\right. \tag{A.16}$$

With $\hat{N}_e = \hat{\omega}^2 - \frac{10}{3}\hat{\omega} + \frac{5}{3}$ we can rearrange the terms as

$$\hat{\omega}^2(1-f_t)\epsilon_n + \hat{\omega}\left(f_t(1-\epsilon_n) - \frac{10}{3}(1-f_t)\epsilon_n\right) + \frac{5}{3}(1-f_t)\epsilon_n + f_t(\eta_e + \frac{5}{3}\epsilon_n - \frac{7}{3}) = 0 \tag{A.17}$$

and just as with the ITG mode we can write the general solution as $\hat{\omega} = \frac{C}{2} \pm \sqrt{\frac{C^2}{4} - D}$ with

$$C = \frac{f_t(1-\epsilon_n) - \frac{10}{3}(1-f_t)\epsilon_n}{(1-f_t)\epsilon_n} \tag{A.18}$$

and

$$D = \frac{\frac{5}{3}(1-f_t)\epsilon_n + f_t(\eta_e + \frac{5}{3}\epsilon_n - \frac{7}{3})}{(1-f_t)\epsilon_n} \tag{A.19}$$

Solving for $\hat{\omega}$ and $\hat{\gamma}$ gives according to [10]

$$\hat{\omega}_r = \frac{10g}{6} - \frac{1}{2}\frac{f_t}{1-f_t}\left(\frac{1}{\epsilon} - g\right) \tag{A.20}$$

and

$$\hat{\gamma} = \sqrt{\frac{f_t(\eta_e - \eta_{eth})}{\epsilon_n(1 - f_t)}} \tag{A.21}$$

where

$$\eta_{eth} = \frac{2}{3} - \frac{f_t}{2(1 - f_t)} + \frac{10\epsilon_n g(1 - f_t)}{9f_t} + \frac{f_t \epsilon_n g}{4(1 - f_t)} + \frac{f_t}{4\epsilon_n g(1 - f_t)} \tag{A.22}$$

Appendix B

Flux calculations

We will here show how to calculate the flux and peaking factors relating to the ion and electron temperatures, much in the same way as we did for particle density in chapter 3.

Ion heat flux

According to [3], the ion heat diffusivity is given by

$$\chi_i = \frac{1}{\eta_i}\left[\eta_i - \frac{2}{3} - (1-f_t)\frac{10\epsilon_n}{9\tau} - \frac{2}{3}f_t\Delta_i\right]\frac{\hat{\gamma}^3\omega_{De}/k_x^2}{(\hat{\omega}_r + 5/3\tau)^2 + \hat{\gamma}^2} \tag{B.1}$$

where

$$\begin{aligned}\Delta_i = \frac{1}{\hat{N}}\Bigg\{|\hat{\omega}|^2\Bigg[|\hat{\omega}|^2(\epsilon - 1) + \hat{\omega}_r\left(\frac{14}{3} - 2\eta_e - \frac{10}{3}\epsilon_n\right) + \frac{5}{3}\left(-\frac{11}{3} + 2\eta_e + \frac{7}{3}\epsilon_n\right) \\ - \frac{5}{3\tau}\left(1 + \eta_e - \frac{5}{3}\epsilon_n\right)\Bigg] + \frac{50}{9\tau}(1-\epsilon_n)\hat{\omega}_r + \frac{25}{9\tau}\left(\eta_e - \frac{7}{3} + \frac{5}{3}\epsilon_n\right)\Bigg\}\end{aligned} \tag{B.2}$$

and

$$\hat{N} = \left(\hat{\omega}_r^2 - \hat{\gamma}^2 - \frac{10}{3}\hat{\omega}_r + \frac{5}{3}\right)^2 + 4\left(\hat{\omega}_r\hat{\gamma} - \frac{5}{3}\hat{\gamma}\right)^2 \tag{B.3}$$

Arranging the term by sign and factoring with regard to $\hat{\omega}_r$, due to the fact that it can change signs, we get

$$\chi_i = \left[1 - \left(A_i\frac{\epsilon_n}{\eta_i} + B_i\frac{\eta_e}{\eta_i} + \frac{C_i}{\eta_i}\right)\right]\frac{\hat{\gamma}^3\omega_{De}/k_x}{(\hat{\omega}_r + 5/3\tau)^2 + \hat{\gamma}^2} \tag{B.4}$$

where

$$A_i = (1-f_t)\frac{10}{9\tau} + \frac{2f_t}{3\hat{N}}\left(|\hat{\omega}|^4 - \frac{10}{3}|\hat{\omega}|^2\hat{\omega}_r + \frac{35}{9}|\hat{\omega}|^2 - \frac{50}{9\tau} + \frac{125}{27}\right) \tag{B.5a}$$

$$B_i = \frac{2f_t}{3\hat{N}}\left(-2|\hat{\omega}|^2\hat{\omega}_r + \frac{10}{3}|\hat{\omega}|^2 - \frac{5}{3\tau}|\hat{\omega}|^2 + \frac{25}{9\tau}\right) \tag{B.5b}$$

$$C_i = \frac{2f_t}{3\hat{N}}\left(-|\hat{\omega}|^4 + \frac{14}{3}|\hat{\omega}|^2\hat{\omega}_r - \frac{55}{9}|\hat{\omega}|^2 - \frac{5}{3\tau}|\hat{\omega}|^2 + \frac{50}{9\tau}\hat{\omega}_r - \frac{175}{27\tau}\right) \tag{B.5c}$$

where $\frac{\epsilon_n}{\eta_i} = 2\frac{L_{T_i}}{L_B}$, $\frac{\eta_e}{\eta_i} = \frac{L_{T_i}}{L_{T_e}}$ and $\frac{1}{\eta_i} = \frac{L_{T_i}}{L_n}$ contain all gradient contributions.

Positive and negative contributions to χ_i

If we write $A_i = A_i^+ + A_i^- + A_i^{\hat{\omega}_r}$, $B_i = B_i^+ + B_i^- + B_i^{\hat{\omega}_r}$ and $C_i = C_i^+ + C_i^- + C_i^{\hat{\omega}_r}$ where

$$A_i^+ = \frac{10}{9\tau} + \frac{2f_t}{3\hat{N}}\left(|\hat{\omega}|^4 + \frac{35}{9}|\hat{\omega}|^2 + \frac{127}{25}\right) \tag{B.6a}$$

$$A_i^- = -\left(\frac{10f_t}{9\tau} + \frac{2f_t}{3\hat{N}}\frac{50}{9\tau}\right) \tag{B.6b}$$

$$A_i^{\hat{\omega}_r} = -\frac{20f_t}{9\hat{N}}|\hat{\omega}|^2\hat{\omega}_r \tag{B.6c}$$

$$B_i^+ = \frac{2f_t}{3\hat{N}}\left(\frac{10}{3}|\hat{\omega}|^2 + \frac{25}{9\tau}\right) \tag{B.6d}$$

$$B_i^- = -\frac{10f_t}{9\hat{N}}|\hat{\omega}|^2 \tag{B.6e}$$

$$B_i^{\hat{\omega}_r} = -\frac{4f_t}{3\hat{N}}|\hat{\omega}|^2\hat{\omega}_r \tag{B.6f}$$

$$C_i^+ = 0 \tag{B.6g}$$

$$C_i^- = -\frac{2f_t}{3\hat{N}}\left(|\hat{\omega}|^4 + \frac{55}{9}|\hat{\omega}|^2 + \frac{175}{27\tau}\right) \tag{B.6h}$$

$$C_i^{\hat{\omega}_r} = \frac{2f_t}{3\hat{N}}\left(\frac{14}{3}|\hat{\omega}|^2 + \frac{50}{9\tau}\right)\hat{\omega}_r \tag{B.6i}$$

Ion heat flux

The ion heat flux is given by $\Gamma_{T_i} = -\chi_i \nabla T_i$ and with χ_i as calculated above we get

$$\frac{R\Gamma_{T_i}}{T_i} = \left[\left(A_i\frac{\epsilon_n}{\eta_i} + B_i\frac{\eta_e}{\eta_i} + \frac{C_i}{\eta_i}\right) - 1\right]\nabla T_i \frac{\hat{\gamma}^3\omega_{De}/k_x}{(\hat{\omega}_r + 5/3\tau)^2 + \hat{\gamma}^2} \tag{B.7}$$

Multiplying this equation with $\frac{R}{T_i}$ gives us the normalized heat flux

$$\frac{R\Gamma_{T_i}}{T_i} = \left[2A_i + B_i\frac{R}{L_{T_e}} + C_i\frac{R}{L_n} - \frac{R}{L_{T_i}}\right]\frac{\hat{\gamma}^3\omega_{De}/k_x}{(\hat{\omega}_r + 5/3\tau)^2 + \hat{\gamma}^2} \tag{B.8}$$

With the separation of positive and negative contributions to χ_i we made above we can easily separate the positive and negative contributions to the heat flux as

$$\frac{R\Gamma_{T_i}^+}{T_i} = \left[2A_i^+ + B_i^+\frac{R}{L_{T_e}} + C_i^+\frac{R}{L_n}\right]\frac{\hat{\gamma}^3\omega_{De}/k_x}{(\hat{\omega}_r + 5/3\tau)^2 + \hat{\gamma}^2} \tag{B.9a}$$

$$\frac{R\Gamma_{T_i}^-}{T_i} = \left[2A_i^- + B_i^-\frac{R}{L_{T_e}} + C_i^-\frac{R}{L_n} - \frac{R}{L_{T_i}}\right]\frac{\hat{\gamma}^3\omega_{De}/k_x}{(\hat{\omega}_r + 5/3\tau)^2 + \hat{\gamma}^2} \tag{B.9b}$$

$$\frac{R\Gamma_{T_i}^{\hat{\omega}_r}}{T_i} = \left[2A_i^{\hat{\omega}_r} + B_i^{\hat{\omega}_r}\frac{R}{L_{T_e}} + C_i^{\hat{\omega}_r}\frac{R}{L_n}\right]\frac{\hat{\gamma}^3\omega_{De}/k_x}{(\hat{\omega}_r + 5/3\tau)^2 + \hat{\gamma}^2} \tag{B.9c}$$

Peaking factors

By setting $\Gamma_{T_i} = 0$ we get an expression for the peaking factor for $\frac{R}{L_{T_i}}$ where

$$\left.\frac{R}{L_{T_i}}\right|_{\Gamma_{T_i}=0} = 2A_i + B_i\frac{R}{L_{T_e}} + C_i\frac{R}{L_n} \tag{B.10}$$

In order to get some sense of scale we investigate the case where the imaginary contribution to $\hat{\gamma}$ is much smaller than the real part $\hat{\omega}_r$, which we will set to ±1. We then get

$$\begin{aligned}\left.\frac{R}{L_{T_i}}\right|_{\hat{\omega}_r=1} &= 2\left[(1-f_t)\frac{10}{9\tau} + \frac{2f_t}{3\hat{N}}\left(\frac{167}{27} - \frac{50}{9\tau}\right)\right] \\ &+\frac{2f_t}{3\hat{N}}\left[\left(\frac{4}{3} + \frac{10}{9\tau}\right)\frac{R}{L_{T_e}} - \left(\frac{52}{9} - \frac{70}{27\tau}\right)\frac{R}{L_n}\right]\end{aligned} \tag{B.11}$$

and

$$\begin{aligned}\left.\frac{R}{L_{T_i}}\right|_{\hat{\omega}_r=-1} &= 2\left[(1-f_t)\frac{10}{9\tau} + \frac{2f_t}{3\hat{N}}\left(\frac{347}{27} - \frac{50}{9\tau}\right)\right] \\ &+\frac{2f_t}{3\hat{N}}\left[\left(\frac{16}{3} + \frac{10}{9\tau}\right)\frac{R}{L_{T_e}} - \left(\frac{106}{9} - \frac{370}{27\tau}\right)\frac{R}{L_n}\right]\end{aligned} \tag{B.12}$$

Electron heat flux

According to [3], the electron heat diffusivity is given by

$$\chi_e = \frac{1}{\eta_e}f_t\left(\eta_e - \frac{2}{3} - \frac{2}{3}\Delta_e\right)\frac{\hat{\gamma}^3\omega_{De}/k_x}{(\hat{\omega}_r - 5/3)^2 + \hat{\gamma}^2} \tag{B.13}$$

where

$$\begin{aligned}\Delta_e = \frac{1}{\hat{N}}\Bigg\{&|\hat{\omega}|^2\left[|\hat{\omega}|^2(\epsilon-1) + \hat{\omega}_r\left(\frac{14}{3} - 2\eta_e - \frac{10}{3}\epsilon_n\right) + \frac{5}{3}\left(-\frac{8}{3} + 3\eta_e + \frac{2}{3}\epsilon_n\right)\right] \\ &+\frac{50}{9}(1-\epsilon_n)\hat{\omega}_r - \frac{25}{9}\left(\eta_e - \frac{7}{3} + \frac{5}{3}\epsilon_n\right)\Bigg\}\end{aligned} \tag{B.14}$$

With the gradient dependency written out we have

$$\chi_e = \left[1 - \frac{2}{3\hat{N}}(A_e\frac{\epsilon_n}{\eta_e} + \frac{B_e}{\eta_i} + C_e)\right]\frac{f_t\hat{\gamma}^3\omega_{De}/k_x}{(\hat{\omega}_r - 5/3)^2 + \hat{\gamma}^2} \tag{B.15}$$

where

$$A_e = |\hat{\omega}|^4 - \frac{10}{3}|\hat{\omega}|^2\hat{\omega}_r + \frac{10}{9}|\hat{\omega}|^2 + \frac{50}{9}\hat{\omega}_r + \frac{125}{27} \tag{B.16a}$$

$$B_e = -|\hat{\omega}|^4 + \frac{14}{3}|\hat{\omega}|^2\hat{\omega}_r - \frac{40}{9}|\hat{\omega}|^2 - \frac{50}{9}\hat{\omega}_r - \frac{175}{27} + \hat{N} \tag{B.16b}$$

$$C_e = 5|\hat{\omega}|^2 - 2|\hat{\omega}|^2\hat{\omega}_r - \frac{25}{9} \tag{B.16c}$$

and $\frac{\epsilon_n}{\eta_e} = 2\frac{L_{T_e}}{L_B}$ and $\frac{1}{\eta_i} = \frac{L_{T_i}}{L_n}$ contain all gradients.

Positive and negative contributions to χ_e

Similar to the case with the ion transport we write $A_e = A_e^+ + A_e^- + A_e^{\hat{\omega}_r}$, $B_e = B_e^+ + B_e^- + B_e^{\hat{\omega}_r}$ and $C_e = C_e^+ + C_e^- + C_e^{\hat{\omega}_r}$ where

$$A_e^+ = |\hat{\omega}|^4 + \frac{10}{9}|\hat{\omega}|^2 + \frac{125}{27} \tag{B.17a}$$

$$A_e^- = 0 \tag{B.17b}$$

$$A_e^{\hat{\omega}_r} = \left(\frac{50}{9} - \frac{10}{3}|\hat{\omega}|^2\right)\hat{\omega}_r \tag{B.17c}$$

$$B_e^+ = \hat{N} \tag{B.17d}$$

$$B_e^- = -\left(|\hat{\omega}|^2(|\hat{\omega}|^2 + \frac{40}{9}) + \frac{175}{27}\right) \tag{B.17e}$$

$$B_e^{\hat{\omega}_r} = \left(\frac{14}{3}|\hat{\omega}|^2 - \frac{50}{9}\right)\hat{\omega}_r \tag{B.17f}$$

$$C_e^+ = 5|\hat{\omega}|^2 \tag{B.17g}$$

$$C_e^- = -\frac{25}{9} \tag{B.17h}$$

$$C_e^{\hat{\omega}_r} = -2|\hat{\omega}|^2\hat{\omega}_r \tag{B.17i}$$

Electron heat flux

Using $\Gamma_{T_e} = -\chi_e \nabla T_e$ we get

$$\frac{R\Gamma_{T_e}}{T_e} = \left[\frac{2}{3\hat{N}}\left(A_e\frac{\epsilon_n}{\eta_e} + \frac{B_e}{\eta_e} + C_e\right) - 1\right]\frac{f_t\hat{\gamma}^3\omega_{De}/k_x}{(\hat{\omega}_r - 5/3)^2 + \hat{\gamma}^2}\nabla T_e \tag{B.18}$$

We normalize by multiplying the equation with $\frac{R}{T_e}$ and get

$$\frac{R\Gamma_{T_e}}{T_e} = \left[\frac{2}{3\hat{N}}\left(2A_e + B_e\frac{R}{L_n} + C_e\frac{R}{L_{T_e}}\right) - \frac{R}{L_{T_e}}\right]\frac{f_t\hat{\gamma}^3\omega_{De}/k_x}{(\hat{\omega}_r - 5/3)^2 + \hat{\gamma}^2} \tag{B.19}$$

We can separate the positive and negative contributions as above

$$\frac{R\Gamma_{T_e}^+}{T_e} = \frac{2}{3\hat{N}}\left[2A_e^+ + B_e^+\frac{R}{L_n} + C_e^+\frac{R}{L_{T_e}}\right]\frac{f_t\hat{\gamma}^3\omega_{De}/k_x}{(\hat{\omega}_r - 5/3)^2 + \hat{\gamma}^2} \tag{B.20a}$$

$$\frac{R\Gamma_{T_e}^-}{T_e} = \left[\frac{2}{3\hat{N}}\left(2A_e^- + B_e^-\frac{R}{L_n} + C_e^-\frac{R}{L_{T_e}}\right) - \frac{R}{L_{T_e}}\right]\frac{f_t\hat{\gamma}^3\omega_{De}/k_x}{(\hat{\omega}_r - 5/3)^2 + \hat{\gamma}^2} \tag{B.20b}$$

$$\frac{R\Gamma_{T_e}^{\hat{\omega}_r}}{T_e} = \frac{2}{3\hat{N}}\left[2A_e^{\hat{\omega}_r} + B_e^{\hat{\omega}_r}\frac{R}{L_n} + C_e^{\hat{\omega}_r}\frac{R}{L_{T_e}}\right]\frac{f_t\hat{\gamma}^3\omega_{De}/k_x}{(\hat{\omega}_r - 5/3)^2 + \hat{\gamma}^2} \tag{B.20c}$$

Peaking factors

By setting $\Gamma_{T_e} = 0$, we get the peaking factor for $\frac{R}{L_{T_e}}$ as

$$\left.\frac{R}{L_{T_e}}\right|_{\Gamma_{T_e}=0} = \frac{2A_e + B_e\frac{R}{L_n}}{\frac{3\hat{N}}{2} - C_e} \tag{B.21}$$

As for $\Gamma_{T_i} = 0$ we investigate the case when $\hat{\omega} = \hat{\omega}_r = \pm 1$ and get

$$\left.\frac{R}{L_{T_e}}\right|_{\hat{\omega}_r=1} = \frac{1}{6}\left(242 - 167\frac{R}{L_n}\right) \tag{B.22}$$

and

$$\left.\frac{R}{L_{T_e}}\right|_{\hat{\omega}_r=-1} = \frac{61}{336} + \frac{39}{84}\frac{R}{L_n} \tag{B.23}$$

Appendix C

Basic particle motion due to electric and magnetic fields

Electric and magnetic fields described by the Maxwell equations

$$\nabla \cdot \mathbf{E} = \frac{\rho}{\epsilon_0} \tag{C.1a}$$

$$\nabla \times \mathbf{E} = -\frac{\partial \mathbf{B}}{\partial t} \tag{C.1b}$$

$$\nabla \cdot \mathbf{B} = 0 \tag{C.1c}$$

$$\nabla \times \mathbf{B} = \frac{1}{c^2}\frac{\partial \mathbf{E}}{\partial t} + \frac{1}{c^2 \epsilon_0}\mathbf{J} \tag{C.1d}$$

play a central role in contributing to the transport of particles in a tokamak, so we will briefly review some simple relations.

The force on a particle is given by the *Lorentz force equation*

$$\mathbf{F} = m\frac{d\mathbf{v}}{dt} = q(\mathbf{E} + \mathbf{v} \times \mathbf{B}) \tag{C.2}$$

We will focus on the effects of a magnetic **B**-field, so we ignore any **E**-field and write (1.3) as

$$\frac{d\mathbf{v}}{dt} = \frac{q}{m}(\mathbf{v} \times \mathbf{B}) \tag{C.3}$$

We assume that $\mathbf{B} = B\hat{\mathbf{z}}$, and since we are only interested in the velocity $\mathbf{v}_\perp$ perpendicular to the magnetic field we also assume that $\mathbf{v}_\perp = (v_x, v_y, 0)$.

This gives us

$$\ddot{v}_x + \big(\frac{qB}{m}\big)^2 v_x = 0 \tag{C.4a}$$

$$\ddot{v}_y + \big(\frac{qB}{m}\big)^2 v_y = 0 \tag{C.4b}$$

We define the cyclotron frequency

$$\omega_c = \frac{|q|B}{m} \tag{C.5}$$

and thus the solutions to (1.5) can be written as

$$v_x = v_\perp \cos(\pm\omega_c t + \varphi_x) \tag{C.6a}$$

$$v_y = v_\perp \cos(\pm\omega_c t + \varphi_y) \tag{C.6b}$$

where $v_\perp$, φ_x and φ_y are constants determined by initial conditions.

Integrating (1.7) and selecting $\varphi_x = 0$, $\varphi_y = \pi/2$ gives us formulas for the positions

$$x = \pm\rho \sin(\pm\omega_c t) \tag{C.7a}$$

$$v = \pm\rho \cos(\pm\omega_c t) \tag{C.7b}$$

where we have defined the *Larmor radius*

$$\rho = \frac{v_\perp}{\omega_c} \tag{C.8}$$

We interpret ρ as the oscillatory deviation from the mean path for a particle in the magnetic field.

Now, we wish to find a general expression for the drift velocity resulting from an additional perpendicular force $\mathbf{F}_\perp$ applied to the mass m by starting out with

$$\frac{d\mathbf{v}_\perp}{dt} = \frac{q}{m}(\mathbf{v}_\perp \times \mathbf{B}) + \frac{\mathbf{F}_\perp}{m} \tag{C.9}$$

we assume that the perpendicular velocity $\mathbf{v}_\perp$ consists of a time dependent and a constant drift part, i.e.

$$\mathbf{v}_\perp(t) = \mathbf{u}(t) + \mathbf{v}_D \tag{C.10}$$

Putting this into (1.10) gives us

$$\frac{d\mathbf{u}}{dt} = \frac{q}{m}\mathbf{u} \times \mathbf{B} + \frac{q}{m}\mathbf{v}_D \times \mathbf{B} + \frac{\mathbf{F}_\perp}{m} \tag{C.11}$$

which includes the expression in (1.9), which we remove leading to

$$\mathbf{v}_D = \frac{1}{q}\frac{\mathbf{F}_\perp \times \mathbf{B}}{B^2} \tag{C.12}$$

Contributions to particle drift in tokamaks

Using equation C.12 for $\mathbf{F}_E = q\mathbf{E}$ and $\mathbf{F}_g = m\mathbf{g}$ gives the *electrostatic drift*

$$\mathbf{v}_E = \frac{\mathbf{E} \times \mathbf{B}}{B^2} \tag{C.13}$$

and the *gravitational drift*

$$\mathbf{v}_g = \frac{m}{q}\frac{\mathbf{g}\times\mathbf{B}}{B^2} \tag{C.14}$$

respectively. Also taking into account the centrifugal force given by $\mathbf{F}_c = \frac{mv_\parallel^2}{R_c^2}\mathbf{R}_c = -\frac{mv_\parallel^2}{B}\nabla|B|$ we get the *curvature drift*

$$\mathbf{v}_c = \frac{mv_\parallel^2}{qB}\frac{\mathbf{B}\times\nabla B}{B^2} \tag{C.15}$$

There are also drifts too complicated to derive here, such as the *polarization drift*

$$\mathbf{v}_{pj} = \frac{1}{B_0\omega_{cj}}\left[\frac{\partial}{\partial t} + \mathbf{v}\cdot\nabla\right]\mathbf{E} \tag{C.16}$$

where B_0 is the background magnetic field and j refers to the particle species, i.e. $j = i$ for ions and $j = e$ for electrons.

Further we have an anisotropic drift

$$\mathbf{v}_{\pi j} = \frac{\hat{z}\times\nabla\cdot\pi_j}{q_j n_j B_0} \tag{C.17}$$

where π_j is the stress tensor, as well as a *diamagnetic drift*

$$\mathbf{v}_{*j} = \frac{\mathbf{B}\times\nabla p_j}{q_j n_j B^2} \tag{C.18}$$

where p_j is the plasma pressure. Finally we also have a drift due to the inhomogeneity of the magnetic field in the tokamak, known as a ∇B *drift*

$$\mathbf{v}_{\nabla B} = \frac{m_j v_\perp^2}{2q_j B}\frac{\mathbf{B}\times\nabla B}{B^2} \tag{C.19}$$

Note that all drift velocities that depend on the charge q will have opposite signs for ions and electrons.

© 2015, Ken Ryrbo